Thiophene- and Selenophene-Based Heteroacenes: Combined Quantum Chemical DFT and Spectroscopic Raman and UV–Vis–NIR Study

ARTICLE *in* THE JOURNAL OF PHYSICAL CHEMISTRY B · AUGUST 2007

Impact Factor: 3.3 · DOI: 10.1021/jp067262t · Source: PubMed

7 AUTHORS, INCLUDING:

Rocio Ponce Ortiz
University of Malaga
69 PUBLICATIONS **2,432** CITATIONS
SEE PROFILE

Shigehiro Yamaguchi
Nagoya University
205 PUBLICATIONS **7,224** CITATIONS
SEE PROFILE

Victor Hernandez
University of Malaga
172 PUBLICATIONS **2,987** CITATIONS
SEE PROFILE

Juan Teodomiro López Navarrete
University of Malaga
334 PUBLICATIONS **5,227** CITATIONS
SEE PROFILE

Thiophene- and Selenophene-Based Heteroacenes: Combined Quantum Chemical DFT and Spectroscopic Raman and UV−Vis−NIR Study

Reyes Malavé Osuna,[†] Rocío Ponce Ortiz,[†] Toshihiro Okamoto,[‡] Yoshitake Suzuki,[‡] Shigehiro Yamaguchi,[‡] Víctor Hernández,[†] and Juan Teodomiro López Navarrete*,[†]

Department of Physical Chemistry, University of Málaga, 29071-Málaga, Spain, and Department of Chemistry, Graduate School of Science, Nagoya University, Furo, Chikusa, Nagoya, 464-8602

Received: November 3, 2006; In Final Form: April 19, 2007

In this article, we report the characterization of a series of thiophene- and selenophene-based heteroacenes, materials with potential applications in organic electronics. In contrast to the usual α-oligothiophenes, these annelated oligomers have a larger band gap than most semiconductors currently used in the fabrication of organic field-effect transistors (OFETs) and therefore they are expected to be more stable in air. The synthesis of these fused-ring molecular materials was motivated by the notion that a more rigid and planar structure should reduce defects (such as torsion about single bonds between α-linked units or S-*syn* defects) and thus improve π-conjugation for better charge-carrier mobility. The conjugational properties of these heteroacenes have been investigated by means of FT-Raman spectroscopy, revealing that π-conjugation increases with the increasing number of annelated rings. DFT and TDDFT quantum chemical calculations have been performed, at the B3LYP/6-31G** level, to assess information regarding the minimum-energy molecular structure, topologies, and absolute energies of the frontier molecular orbitals around the gap, vibrational normal modes related to the main Raman features, and vertical one-electron excitations giving rise to the main optical absorptions.

I. Introduction

Fused polycyclic aromatic hydrocarbons (PAHs) are an important class of molecules as fundamental skeletons for functional organic materials.[1] Their rigid π-conjugated frameworks, free from conformational disorder, are a decisive characteristic leading to unique electronic properties. A representative example is a linearly fused acene such as pentacene.[2,3] The flat π-conjugated framework realizes densely packed solid-state structures that are beneficial in achieving high carrier mobility. This class of molecules is currently among the most extensively investigated materials for organic thin film transistors.[4] In this context, thiophene- and selenophene-based heteroacenes are also of interest,[5−9] since the heteroatom effects not only the electronic structures but also the solid-state structures[10] would make them more attractive candidates. However, only a limited number of this class of molecules have been reported to date, such as dibenzo-annulated dithieno[3,2-*b*:2′,3′-*d*]thiophene,[5] fused oligothiophenes consisting of five or seven thiophene rings,[6,7] and a fully fused polythiophene.[8] This may be due to a lack of useful synthetic routes in terms of efficiency as well as accessible structural diversity. The exploration of conceptually new methodology is thus a compelling subject in this chemistry.

Some of us have recently reported on a general and facile synthesis of thiophene- and selenophene-containing heteroacenes in good yields on the basis of an intramolecular triple cyclization of bis(*o*-haloaryl)diacetylenes in a regiospecific manner.[11] All these heteroacenes are very stable toward heat and light and can be handled without special care. Furthermore, these annelated systems have a larger band gap than most semiconducting materials used in organic field-effect transistors (OFETs) and therefore they are expected to have improved environmental stability.

Molecular spectroscopy is a fundamental tool to establish structure−property relationships guiding the design of new and improved molecular materials. In particular, Raman spectroscopy is very well suited for the study of conjugated systems. Raman frequencies and intensities are experimental observables emerging directly from the π-conjugated frame which account for the most important electronic signatures of oligothiophenes. The *effective conjugation coordinate* (ECC) model[12] predicts two main trends for the Raman spectral profiles of π-conjugated molecules: (a) selective enhancement of particular scatterings associated with collective C═C/C−C stretching vibrations of the π-conjugated backbone (this phenomenon relates to the occurrence in these types of one-dimensional systems of an electron−phonon mechanism which is at the origin of their outstanding optical and electrical features); (b) frequency downshift of these enhanced Raman bands upon relaxation of the molecular structure as the consequence of either greater π-electron conjugation in the neutral state or quinoidization induced by ionization. When these experimental spectroscopic data are combined with reliable quantum chemical calculations, it is possible to assess precisely the relevant molecular parameters which would be very difficult to evaluate by other conventional experimental techniques. First principles quantum chemical calculations in the framework of the density functional theory (DFT) are very well suited to model extended π-conjugated systems due to implemented electron-correlation effects.

In this contribution we use Raman spectroscopy to analyze the conjugational properties of a series of thiophene- and

* To whom correspondence should be addressed. E-mail: teodomiro@uma.es.
[†] University of Málaga.
[‡] Nagoya University. E-mail: yamaguchi@chem.nagoya-u.ac.jp (S.Y.).

10.1021/jp067262t CCC: $37.00
Published on Web 06/12/2007

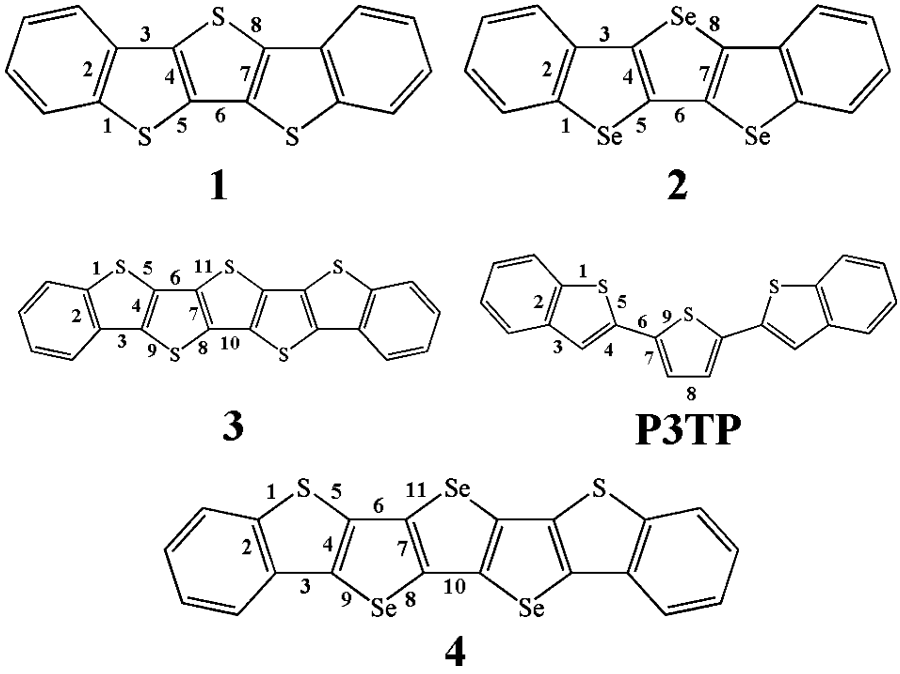

Figure 1. Chemical structures and abbreviated notation of the thiophene- and selenophene-based heteroacenes studied in this work and the theoretical model for comparison, P3TP (bond numbering used for Table 2).

selenophene-based heteroacenes and investigate their optical properties by means of UV−vis−NIR absorption spectroscopy. The whole set of experimental data has been interpreted with the help of DFT and time-dependent DFT (TDDFT) quantum chemical calculations, at the B3LYP/6-31G** level, regarding the minimum-energy molecular structure, topologies, and absolute energies of the frontier molecular orbitals (MOs) around the gap, vibrational normal modes associated with the most outstanding Raman scatterings, and one-electron vertical excitations involved in the main optical absorptions.

II. Experimental and Theoretical Details

Synthesis and purification of the thiophene- and selenophene-based heteroacenes were described elsewhere.[11] Chemical structures and abbreviated notation of the four systems under study are depicted in Figure 1. Characterizations of compounds **3** and **4** were carried out by means of solid-state ^{13}C NMR spectroscopy (JEOL JNM-ECA500; see Figures S1 and S2 in the Supporting Information) and elemental analysis.[11] We also attempted to measure the melting points for these compounds. However, according to the TGA (Seiko TGA 6200 at a heating rate of 5 °C/min under nitrogen) and DSC (Seiko DSC 6200 at a heating rate of 10 °C/min under a stream of nitrogen) measurements, decomposition temperatures with a 5% weight loss (Td5) are 374 and 411 °C for **3** and **4**, respectively, and both compounds do not melt below the Td5 (see Figures S3 and S4 in the Supporting Information). UV−vis absorption spectra were recorded with a Shimadzu UV-3150 spectrometer using degassed spectral grade THF (TCI Co.) as received with a sufficiently low concentration ($<10^{-6}$ M). Emission spectra were measured using a JASCO FP-750 spectrofluorometer. No fluorescent contaminants were detected upon excitation in the wavelength region of experimental interest. Solutions for emission measurements were prepared with an absorbance in the visible spectral region between 0.1 and 0.2. The measurements of the UV−vis absorption and fluorescence spectra for compounds **3** and **4** were conducted using pure samples obtained by sublimation (compound **3**, 320 °C/0.15 mmHg; compound **4**, 320 °C/0.2 mmHg).

Fourier transform infrared absorption (FT-IR) spectra were recorded on a Bruker Equinox 55 spectrometer. Compounds were ground to a powder and pressed in KBr pellets. FT-IR spectra, with a spectral resolution of 2 cm^{-1}, were collected by averaging 50 scans. Interference from atmospheric water vapor was minimized by purging the instrument with dry argon before starting the data collection. FT-Raman scattering spectra were collected on a Bruker FRA106/S apparatus and a Nd:YAG laser source ($\lambda_{exc} = 1064$ nm), in a back-scattering configuration. The operating power for the exciting laser radiation was kept to 100 mW in all the experiments. Samples were analyzed as pure solids in sealed capillaries. Typically, 1000 scans with 2 cm^{-1} spectral resolution were averaged to optimize the signal-to-noise ratio.

Density functional theory (DFT) calculations were carried out by means of the Gaussian 03 program[13] running on SGI Origin 2000 supercomputer. Becke's three-parameter exchange functional combined with the LYP correlation functional (B3LYP)[14] was employed because it has been shown that the B3LYP functional yields similar geometries for medium-sized molecules as MP2 calculations do with the same basis sets.[15,16] Moreover, the DFT force fields calculated using the B3LYP functional yield infrared spectra in very good agreement with experiments.[17,18] The standard 6-31G** basis set was used to obtain optimized geometries on isolated entities.[19] C_{2v} symmetry constraints were imposed during the geometry optimization of each system (namely, all geometrical parameters of half the molecule were allowed to vary independently except for the planarity of fused rings). On the resulting ground-state optimized geometries, harmonic vibrational frequencies, and infrared and Raman intensities were calculated with the B3LYP functional.

We used the often-practiced adjustment of the theoretical force fields in which calculated harmonic vibrational frequencies are uniformly scaled down by a factor of 0.96 for the 6-31G** calculations, as recommended by Scott and Radom.[17] This scaling procedure is often accurate enough to disentangle serious experimental misassignments. All quoted vibrational frequencies reported in the paper are thus scaled values. The theoretical spectra were obtaining by convoluting the scaled frequencies

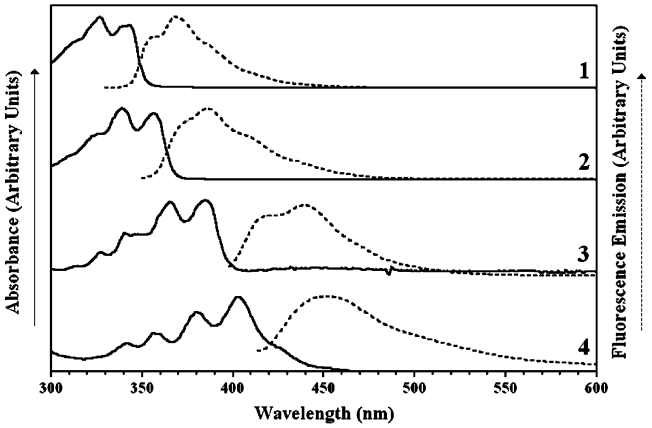

Figure 2. Normalized UV−vis−NIR absorption (solid line) and fluorescence emission (dotted line) spectra of **1**−**4** in THF. (The spectra of **1** and **2** were collected at room temperature, whereas those for **3** and **4** were recorded upon heating due to their low solubility.)

TABLE 1: UV−Vis Absorption Maxima (λ_{max}) of 1−4

compd	λ_{max} in nm (log ϵ)[a]
1	343 (4.51), 327 (4.56), 313 (4.37); 338 (4.49); 261 (4.30), 253 (4.26)
2	357 (4.56), 339 (4.59), 325 (4.39), 309 (4.09); 271 (4.14), 262 (4.13), 251 (4.17)
3	385, 366, 341, 327
4	404, 380, 357, 342

[a] log ϵ values for **3** and **4** were not determined due to their low solubility.

with Gaussian functions (10 cm^{-1} width at the half-height). The relative heights of the Gaussians were determined from the theoretical Raman scattering activities.

Vertical electronic excitation energies were computed by using the time-dependent DFT (TDDFT) approach.[20,21] The 20 lowest-energy electronic excited states were computed for all the molecules. The computational cost of TDDFT is roughly comparable to that of single-excitation theories based on an HF ground state, such as single-excitation configuration interactions (CIS). Numerical applications reported so far indicate that TDDFT formalism employing current exchange-correlation functionals performs significantly better than HF-based single excitation theories for the low-lying valence excited states of both closed-shell and open-shell molecules.[22,23] TDDFT calculations were carried out using the B3LYP functional and the 6-31G** basis set on the previously optimized molecular geometries obtained at the same level of calculation. Molecular orbital contours were plotted using Molekel 4.3.[24]

III. Results and Discussion

A. UV−Vis Absorption Data. Figure 2 displays the normalized electromagnetic absorption and emission spectra of the four systems under study. All the heteroacenes show a strong electromagnetic absorption in the visible with the lowest energy absorption maxima around 340−420 nm and a second weak band at higher energy. Well-resolved vibronic structures, due to the planar and rigid structure of the heteroacenes, are evident in all the UV−vis−NIR absorption spectra (the precise wavelengths of the various vibronic peaks of each optical absorption are provided in Table 1 together with the corresponding log ϵ values). The optical absorptions red-shift upon increasing the number of fused rings, with a commesurate intensity increase for the longest wavelength band. We also observe that **1** and **3** show absorption maxima similar to those of α-bithiophene and α-terthiophene, in spite of the higher number of sulfur linkages and the phenyl units flanking the heterocyclic core: an indication that the number of double bonds in the oligothienyl scaffold in each mainly dictates this property. In addition, the electromagnetic absorption envelope is found to be significantly narrower for the thiophene-based heteroacenes than for the nonfused α-oligothiophenes with the same number of double bonds in the oligothienyl frame; furthermore, the vibronic peaks are much more clearly distinguishable for the former set of compounds, consistent with absorption from a single molecular conformation in solution. However, contrary to the absorption maxima of **1** and **3** similar to those of the nonfused α-oligothiophenes, the fluorescence emissions of the former compounds are significantly blue-shifted with respect to those measured for the latter ones. Consequently, the Stokes shift is smaller for the heteroacenes, consistent with a closer geometric match between the ground state and the first singlet excited state for these systems. Finally, we also observe that the further extension of the π-conjugated backbone through the addition of two terminal benzene rings to the oligothienyl core of **3** causes a red-shift of the lowest energy absorption maximum by near 40 nm with respect to the corresponding quinquethienoacene lacking of end-fused benzene rings.[7]

TABLE 2: B3LYP/6-31G Values (in Å) for Selected Skeletal Bond Lengths of 1−4[a]**

bond no.	**1**	**2**	**3**	**4**	P3TP
1	1.773	1.900	1.773	1.772	1.756
2	1.421	1.419	1.421	1.421	1.418
3	1.435	1.435	1.434	1.432	1.432
4	1.387	1.381	1.387	1.384	1.372
5	1.754	1.883	1.754	1.756	1.772
6	1.419	1.415	1.418	1.417	1.448
7	1.387	1.381	1.397	1.391	1.383
8	1.754	1.884	1.753	1.884	1.411
9			1.757	1.883	1.752
10			1.417	1.414	
11			1.756	1.885	

[a] For bond numbering, please see Figure 1.

B. Optimized Geometries and Theoretical Electronic Transitions. To gain a deeper insight into the molecular structure in these heteroacenes, geometry optimizations were performed within the framework of the density functional theory, for **1**−**4** and *all-syn*-P3TP using B3LYP/6-31G** model chemistry (Table 2 summarizes the optimized distances for selected skeletal bonds of the five systems). The optimized geometries reveal that the various five-membered rings of a given thiophene- and/or selenophene-based heteroacene display similar C_α=C_β and C_β−C_β bond lengths except for the outermost C_α=C_β bonds fused to the phenyl ring at each side end of the oligomeric chain, which are the longest C=C bond lengths of the whole π-conjugated scaffold. This effect could be attributed to less efficient π-conjugation from the middle of the oligomer chain toward its ends. The DFT//B3LYP/6-31G** calculations predict nearly the same geometry for **1** and **3**, and consequently, the geometric parameters are expected to quickly reach saturation upon chain-lengthening (i.e., this theoretical result can be related to the presence of many electron-rich sulfur and/or selenium atoms surrounding a highly polarizable π-conjugated frame of alternating C=C/C−C bonds). The mean single−double CC bond-length-alternation (BLA) parameter, related to the difference between the average lengths of single and double π-conjugated CC bonds, steadily decreases from 0.030 to 0.020 Å in going from the outer thienyl rings toward the central one in **3**.

TABLE 3: TDDFT//B3LYP/6-31G Vertical One-Electron Excitations (Values in nm) Related to the Strongest UV−Vis Absorptions of the Four Heteroacenes**

compd	exptl[a]	TDDFT//B3LYP/6-31G**	descriptn[b]
1	343 (327, 313)	329 ($f = 0.69$)	H → L
	338	319 ($f = 0.07$)	H − 1 → L
	261 (253)	290 ($f = 0.03$)	H − 2 → L
2	357 (339, 325, 309)	340 ($f = 0.57$)	H → L
	271 (262, 251)	307 ($f = 0.09$)	H − 2 → L
3	385 (366)	380 ($f = 1.20$)	H → L
	341	333 ($f = 0.08$)	H − 1 → L
	327	318 ($f = 0.04$)	H − 2 → L
4	404 (380)	393 ($f = 1.10$)	H → L
	357	352 ($f = 0.09$)	H − 1 → L
	342	332 ($f = 0.05$)	H − 2 → L

[a] Values within parentheses correspond to vibronic peaks. [b] L denotes the LUMO, whereas H, H − 1, and H − 2 denote the HOMO, HOMO-1, and HOMO-2, respectively.

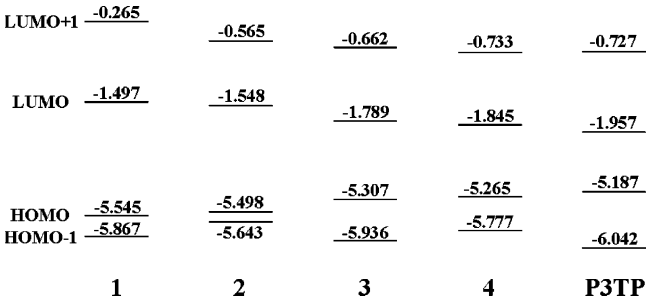

Figure 3. Comparison between the DFT//B3LYP/6-31G** energy levels around the band gap region for **1**−**4** and a P3TP model counterpart with the same number of double bonds as **3**.

To provide insight into the nature of the UV−vis absorptions observed experimentally for the chromophores, the lowest energy electronic excited states of **1**−**4** were calculated at the B3LYP/6-31G** level using the TDDFT approach on their previously optimized ground-state molecular geometries. Transition energies and oscillator strengths are listed in Table 3 along with the description of the experimental absorptions in terms of the dominant one-electron vertical excitations. Figure 3 sketches a comparative diagram with the B3LYP/6-31G** energies of the frontier molecular orbitals around the gap for **1**−**4** and *all-syn*-P3TP, whereas Figure 4 shows the topologies of selected MOs of the four heteroacenes under study, as a guide to the TDDFT analysis of the optical absorptions of these fused systems (i.e., the topologies of the corresponding MOs of *all-syn*-P3TP are provided in Figure S5 in the Supporting Information).

Theoretical calculations predict the appearance in each case of a very strong electronic transition in the visible region, together with two other close but weaker optical transitions (see Table 3). The absorption bands, measured in THF solution at 343 nm (**1**), 357 nm (**2**), 385 nm (**3**), and 404 nm (**4**), correspond to the excitation to the first singlet excited state, which is computed at 329 nm for **1** (with a oscillator strength, *f*, of 0.69), at 340 nm for **2** ($f = 0.57$), at 380 nm for **3** ($f = 1.20$), and at 393 nm for **4** ($f = 1.10$). This vertical transition is mainly described by a one-electron excitation from the highest occupied molecular orbital (HOMO) to the lowest unoccupied molecular orbital (LUMO). Thus, TDDFT model chemistry reproduces, with very good accuracy, the experimental wavelengths for the optical transitions of the four heteroacenes under study and nicely accounts also for the red-shift of the $\pi-\pi^*$ transition in passing either from the shorter systems to the longer ones or upon the replacement of the sulfur atoms by selenium.

Both the HOMO and LUMO of the four heteroacenes are of π-nature and mainly spread over the whole frame of fused heterocycles, with a smaller contribution by part of the phenyl end rings (see Figure 4). As for the HOMO, the C═C bonds are π-bonding and have an alternating phase with respect to their adjacent C═C bonds, whereas, for the LUMO, the C═C bonds are π-antibonding and the $C_\beta-C_{\beta'}$ and $C_\alpha-C_{\alpha'}$ are bonding reminiscent of a quinoidal form. As can be seen in Figure 4, the topologies of these two frontier MOs in the heteroacenes are almost identical with those commonly found in the nonfused α-oligothiophenes. From Figure 3, one can also observe that there occurs a destabilization/stabilization of the HOMO/LUMO terms by 0.047/0.051 eV on going from **1** and **2**, which might account for the red-shift of the lowest energy absorption in the UV−vis spectrum in passing from the former system to the latter one. A similar discussion can be formulated for **3** and **4**; the replacement of the three innermost sulfur atoms by selenium leads to a destabilization/stabilization of the HOMO/LUMO energy levels by 0.042/0.056 eV. Furthermore, from the comparison between the B3LYP/6-31G** energy levels around the band gap region for **3** and the *all-syn*-P3TP model system sketched in Figure 3, it can be concluded that the introduction of two sulfur linkages between the inner β-positions of the α-terthienyl core leads to a stabilization of the HOMO by 0.120 eV and a destabilization of the LUMO by 0.168 eV, so that the overall effect is an increase in the energy gap from 3.230 eV in *all-syn*-P3TP to 3.518 eV in **3**. Finally, upon the addition of the two fused benzene end rings to the quinquethienyl backbone of **3**, the energy of the HOMO level remains nearly unaffected whereas the LUMO level is stabilized by 0.26 eV, in agreement with the experimental redshift of the HOMO → LUMO transition in passing from the quinquethienoacene without fused benzene end rings to **3**.[7]

As aforementioned, TDDFT//B3LYP/6-31G** calculations also predict the appearance of other two weak absorptions quite close in energy to the HOMO → LUMO transition (see Table 3). Thus, the HOMO-1 → LUMO vertical one-electron transition is predicted to occur at at 319 nm for **1** ($f = 0.07$), at 342 nm for **2** ($f = 0.07$), at 333 nm for **3** ($f = 0.08$), and at 352 nm for **4** ($f = 0.09$), whereas the HOMO-2 → LUMO excitation should be observed at around 290 nm for **1** ($f = 0.03$), 307 nm for **2** ($f = 0.09$), 318 nm for **3** ($f = 0.04$), and 332 nm for **4** ($f = 0.05$). Figure 4 shows that the atomic orbital composition of the HOMO-1 in the four fused systems significantly differs from that in common α-oligothiophenes, being mainly concentrated in the heteroacenes over the innermost five-membered heterocycles and with the greatest contribution now coming from the electron-rich sulfur and selenium atoms (i.e., this different topology could justify the closer proximity of the HOMO-1 to the band gap region in the heteroacenes). On the other hand, as mentioned above, the LUMO spreads over the entire frame of π-conjugated C═C/C−C bonds. Consequently, in view of the topologies of the MOs involved in the HOMO-1 → LUMO transition, certain electron density transfer from the heteroatoms toward the π-conjugated core can be expected to take place upon excitation of these oligothienoacenes at near 300 nm.

The experimental oscillator strengths, f_{expt}, for the optical absorptions of **1** and **2** at near 350 nm were estimated from the conversion between extinction coefficient and oscillator strength, $f = 4.319 \times 10^{-9}$ (M cm^2) A, where A is the integrated absorption coefficient. The value of A is found by determining the area under an absorption band that is displayed as x-axis = wavenumber (cm^{-1}) against y-axis = molar absorption coefficient (M^{-1} cm^{-1}). The units of A (M^{-1} cm^{-2}) and the value

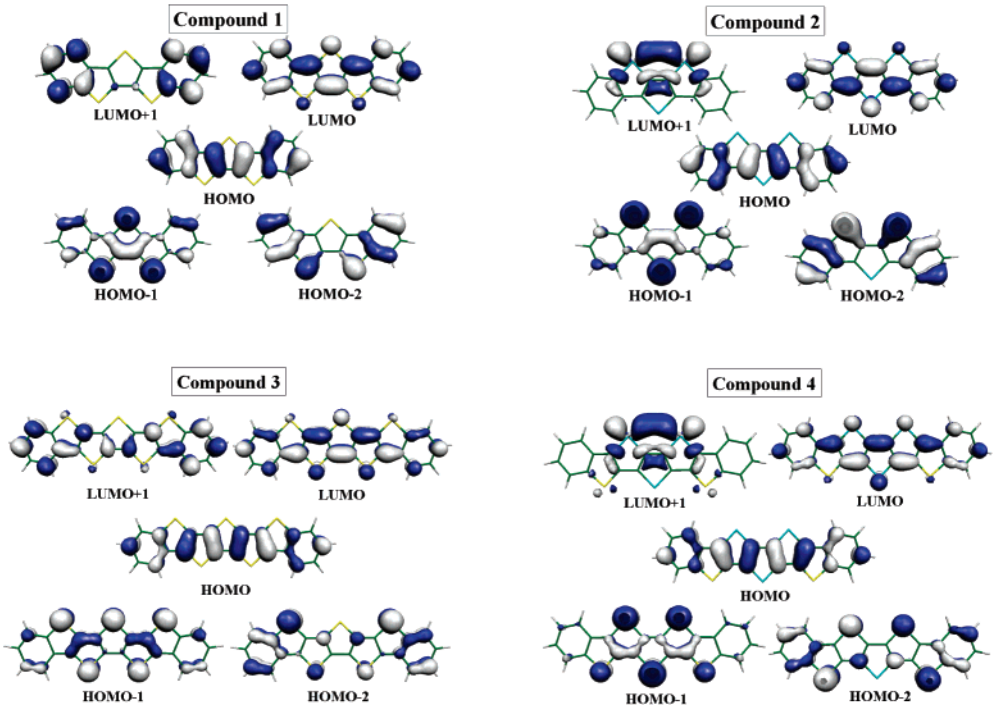

Figure 4. DFT//B3LYP/6-31G** electronic density contours (0.03 e/bohr^3) for selected MOs of **1**−**4**.

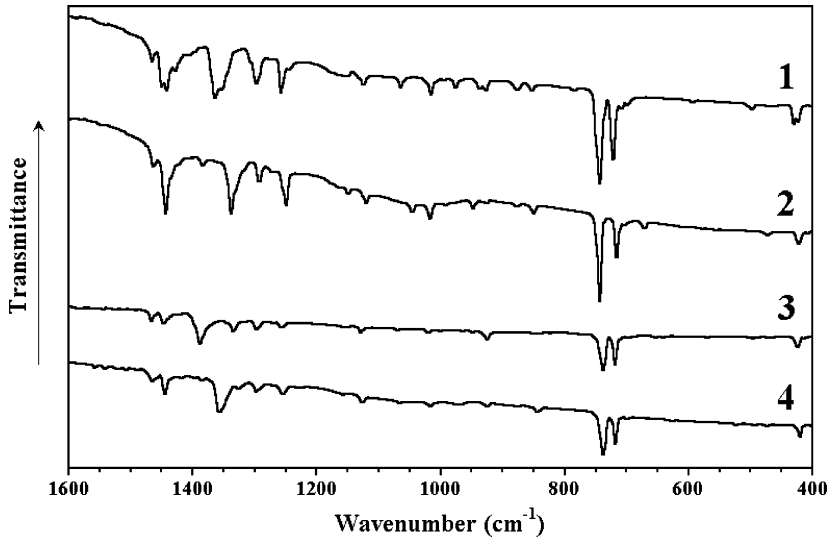

Figure 5. FT-IR spectra of **1**−**4** in the 1600−400 cm^{-1} range.

4.319×10^{-9} M cm^2 cancel to give the dimensionless value of f_{expt}. The accurate estimate of the integrated absorption coefficients for **1** and **2** led to $f_{expt} \approx 0.63$ and 0.66 for the former and latter heteroacenes, respectively, which are in reasonably good agreement with the sum of the oscillator strengths for the two lowest lying calculated transitions of each system as quoted in the paragraphs above, $f_{calc} = 0.76$ for **1** and 0.64 for **2**, which provides another piece of evidence for the quality of the TD-DFT calculations.

C. Experimental and Theoretical Vibrational Spectra. Figures 5 and 6 display the solid-state FT-IR and FT-Raman spectral profiles recorded for **1**−**4**, respectively, whereas Figure 7 serves to illustrate the selective enhancement of some of the skeletal Raman-active vibrations of **3** appearing between 1600 and 1400 cm^{-1}. Finally, Figures 8 and 9 depict the B3LYP/6-31G** vibrational eigenvectors related to the main IR and Raman features, respectively, while Figure 10 shows the dependence with the chain length of the B3LYP/6-31G** Raman spectrum in passing from **1** to **3**.

From the earliest studies on electrically conducting polymers, vis−NIR electronic absorption and infrared and Raman vibrational spectroscopies have been widely used to characterize many different types of π-conjugated systems, both oligomers and polymers, and among them Raman spectroscopy has been shown to be of great help in (i) analyzing the effectiveness of the π-conjugation along a homologous series of oligomers,[25−27] (ii) characterizing different types of conjugational defects induced by either chemical doping or photoexcitation,[28] and (iii) estimating the degree of intramolecular charge transfer in push−pull π-conjugated chromophores.[29,30]

The observation of a limited number of overwhelmingly strong Raman scatterings, even for systems having complex chemical structures,[27f,28f] was definitively accounted for over 20 years ago by Zerbi and co-workers through the development

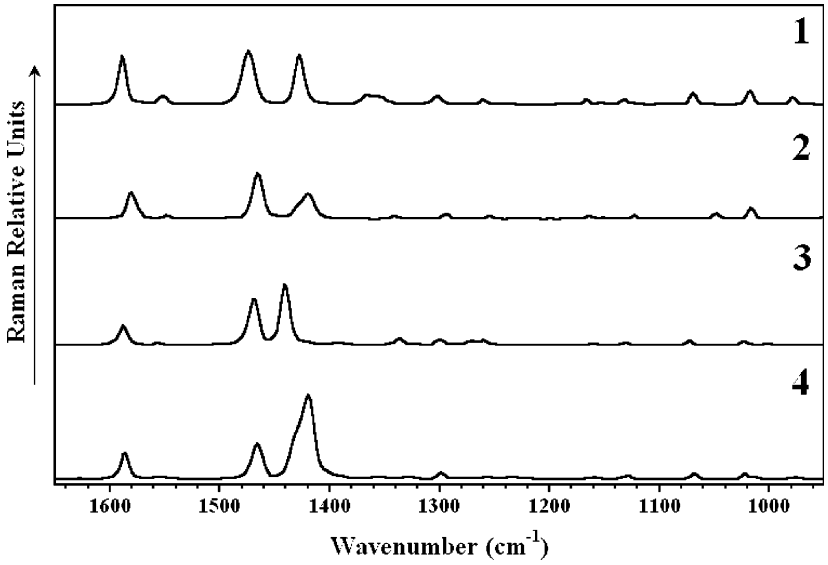

Figure 6. Solid-state FT-Raman spectra of **1**−**4**. The Nd:YAG laser excitation (λ_{exc}) wavelength was 1064 nm.

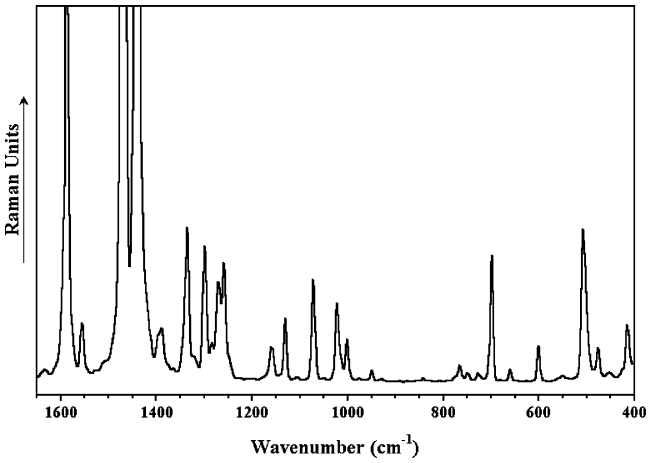

Figure 7. Enlarged profile of the FT-Raman spectrum of **3**, recorded on the pure solid sample, showing the selective enhancement between 1600 and 1400 cm^{-1} of a few scatterings related to specific skeletal stretching modes with respect to the many Raman-active vibrations appearing below 1400 cm^{-1}.

of the *effective conjugation coordinate* (ECC) model. This model, which is now well-accepted, postulates the existence of a unique collective C═C/C−C stretching mode strongly involved in the electron−phonon coupling mechanism which characterizes these one-dimensional π-conjugated chains.[12] In heteroaromatic polyconjugated systems, the so-termed *collective ECC coordinate* has the analytic form of a linear combination of ring C═C/C−C stretchings, which point in the direction from a benzenoid structure (usually that of the ground electronic state) to a quinonoid one (that corresponding to the electronically excited state). The ECC formalism states that the totally symmetric C═C/C−C stretching modes entering in the lattice dynamics of the ECC vibrational coordinate, that is those which give rise to the few and selectively enhanced Raman features, should undergo large dispersions both in peak position and intensity on increasing conjugation length along a given set of neutral oligomers. Thus, changes in Raman frequencies and relative intensities with increasing chain length are particularly useful in evaluating the mean conjugation length for a given family of π-conjugated compounds. Furthermore, upon chemical or electrochemical oxidation/reduction of these π-conjugated heteroaromatic systems, various types of quinonoid-like charged defects are created.[31] The subsequent quinoidization of the

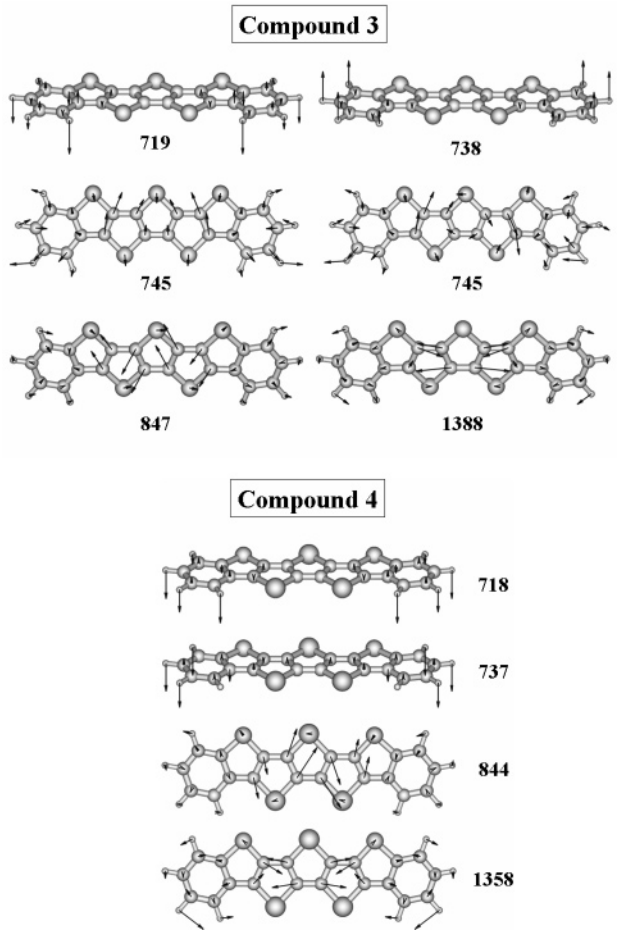

Figure 8. B3LYP/6-31G** vibrational eigenvectors related to some of the strongest IR bands of **3** and **4**. (Experimental frequencies are given in cm^{-1}.)

π-conjugated backbone gives rise to a further red-shift of the strongest Raman lines due to the progressive softening of the conjugated C═C bonds, which is a marker of the type of charged defects created upon oxidation or reduction.[25−28]

Figure 6 shows for these heteroacenes, and particularly for the two longest ones, the usual simplicity of the Raman profiles commonly found in many types of π-conjugated oligomers, as compared with their rather more complex IR absorption spectra.

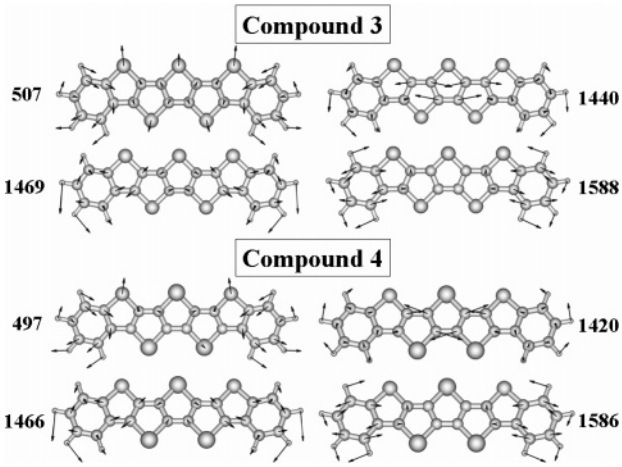

Figure 9. B3LYP/6-31G** vibrational eigenvectors associated with the most outstanding Raman features of **3** and **4**. (Experimental frequency values are given in cm^{-1}.)

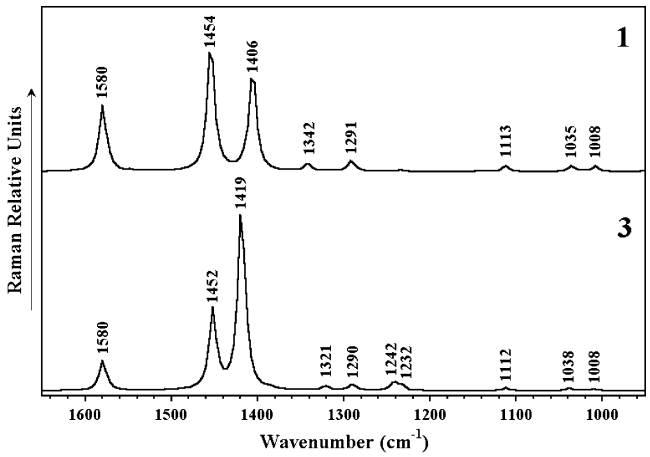

Figure 10. B3LYP/6-31G** Raman spectral profiles computed for **1** and **3**.

Thus, while the former display three main Raman scatterings strongly enhanced with respect to the very many Raman-active vibrations (see Figure 7) at 1588, 1469, and 1440 cm^{-1} for **3** and at 1586, 1466, and 1420 cm^{-1} for **4**, due to ν(C═C) stretching modes, the latter show several features below 1100 cm^{-1}, most of them (i.e., as the strong IR absorptions of **3** and **4** near 740 and 720 cm^{-1} due to out-of-plane γ(C−H) bending modes) being fully decoupled from the π-electron degrees of freedom. On the other hand, B3LYP/6-31G** calculations also show that the outstanding IR absorptions recorded at 1388 cm^{-1} for **3** and 1356 cm^{-1} for **4** arise in each case from a $\nu(C_\beta-C_\beta)$ stretching mode mostly located on the three innermost heterocycles, for which the motions of the adjacent fused rings take place with opposite phases (see Figure 8), so that this skeletal mode is very weakly coupled with the delocalization of the π-electrons over the whole molecular backbone and consequently it displays a vanishing intensity in the Raman spectrum.

Table 4 summarizes the solid-state Raman peak frequencies of the four heteroacenes under study. The strongest Raman scatterings are by far those measured at 1588, 1469, and 1440 cm^{-1} for **3** and at 1586, 1466, and 1420 cm^{-1} for **4** (i.e., their selective enhancement among the very many Raman-active vibrations can be observed in the enlarged profiles depicted in Figure 7). The B3LYP/6-31G** vibrational eigenvectors plotted in Figure 9 show that (i) the scattering near 1590 cm^{-1} is due to a totally symmetric (TS) ν(C═C) stretching mode almost exclusively located on the phenyl end rings, (ii) the feature at

TABLE 4: Peak Positions of the Strongest Solid-State Raman Scatterings for the Four Heteroacenes under Study (Values in cm^{-1})

1	2	3	4
1589	1580	1588	1586
1552	1549	1556	1553
1474	1466	1469	1466
1428	1420	1440	1420
1366			
1355	1340	1336	
1302	1294	1300	1298
		1270	
1260	1254	1259	
1166	1163	1164	
1132	1123	1131	1129
1069	1048	1072	1068
1017	1016	1023	1022
978	948	947	950
788			
709	673	699	699
507	409	507	497

1470 cm^{-1} arises instead from a TS ν(C═C) stretching mode mostly located on the outermost thienyl unit at each side of the oligomeric chain, although largely mixed with a ν(C═C) vibration of the phenyl end rings, and (iii) the strongest Raman scattering at 1440 cm^{-1} (**3**) or 1420 cm^{-1} (**4**) is due to a TS ν_{sym}(C═C) stretching mode of the three innermost heterocyclic units, along which all the inner C═C bonds shrink or lengthen in-phase. Thus, DFT force field calculations evidence that the latter two Raman lines are to be correlated with the characteristic lines A and B, respectively, of the nonfused α-oligothiophenes.[24−26] In view of the eigenvectors plotted in Figure 9, it becomes apparent that the structural changes taking place in the π-conjugated frame along these three molecular vibrations look alike those occurring upon the HOMO → LUMO one-electron vertical excitation. Finally, we observe that the Raman feature measured near 500 cm^{-1} for **3** and **4** also displays a somewhat stronger intensity than in common α-oligothiophenes; its associated eigenvector shows that it is mainly due to a TS δ_{ring} in-plane bending mode with a pronounced collective character, along which all the C−S or C−Se bonds shrink or lengthen in-phase and with similar amplitudes. Its selective enhancement with respect to the huge number of Raman-active normal modes predicted by the optical selection rules suggests that a major role is played by the sulfur of selenium atoms in the π-conjugation of these heteroacenes. In this regard, we also highlight that the two strongest Raman lines A and B are recorded at lower wavenumbers in the heteroacenes than in their nonfused α-oligothienyl counterparts (for instance, lines A and B are measured at 1530 and 1460 cm^{-1} for **3T** and at 1515 and 1459 cm^{-1} for **4T**, respectively), as a molecular signature of the improved π-conjugation in these heteroacenes due to the higher number of heteroatoms which likely translates into a softer and more polarizable π-conjugated frame. Finally, we also observe from the comparison between the FT-Raman spectra of **3** and its fused quinquethienyl counterpart without terminal benzene rings that lines A and B slightly upshift by around 3 cm^{-1} in passing from the former to the latter heteroacene, as a consequence of the more extented π-conjugated path of **3**.[7]

The intensity pattern of the three more selectively enhanced TS ν(C═C) modes of **1** and **3** is also nicely accounted for by DFT//B3LYP/6-31G** model chemistry, as shown in Figure 10, although the theoretical wavenumbers are lower than the experimental ones for both systems (i.e., this mismatch could be ascribed to the well-known tendency of B3LYP/6-31G** data to overestimate π-conjugation). It seems, however, that the peak position of the Raman scattering near 1440 cm^{-1} has not

reached saturation for **3**, but it will continue to red-shift with increasing number of thienyl units in the fused planar backbone so that longer oligothienoacenes could still display better π-conjugational properties than **3**. The further downward dispersion, with a commesurate intensity increase, of the strongest Raman scattering from 1440 cm^{-1} in **3** to 1420 cm^{-1} in **4** upon the replacement of the three innermost sulfur atoms by selenium is also in line with this expectation.

IV. Summary and Conclusions

This work presents an analysis of the molecular scale structural and electronic properties of four thiophene- and selenophene-based heteroacenes with potential applications in organic electronics. Their analysis is performed by combining a selection of spectroscopic tools (electromagnetic absorption, fluorescence emission, and FT-IR and FT-Raman vibrational spectroscopies) with DFT and TDDFT quantum chemical calculations.

The Raman spectroscopic study of these molecular materials provides analysis within the framework of the ECC theory thus allowing for the disection of the key Raman features most prominent in overall π-conjugation. Importantly, the collective characters of both the ECC-related vibrational normal modes and the frontier molecular orbital wave functions (i.e., HOMO and LUMO) primarily determine the optical and electronic properties of this class of heteroacenes. In this regard, DFT calculations performed on a linear α-terthienyl suited model system bearing two fused phenyl end rings, having the same number of π-conjugated double bonds as the quinquethienoacene **3**, show that the bridging of the various inner β-positions of the α-oligothienyl core by sulfur linkages stabilizes the HOMO and destabilizes the LUMO, leading to a broader energy gap than that of the corresponding nonfused oligothienyl counterpart.

These heteroacenes, like many other types of π-conjugated oligomers, display a rather simple Raman spectral profile. DFT calculations allowed identification of the vibrations associated with each of the strongest Raman features selectively enhanced by the occurrence of effective π-conjugation. These totally symmetric vibrations are spread over the whole π-conjugated frame indicating their collective character. Furthermore, careful comparison between the FT-Raman spectral profiles of these heterocenes and the nonfused α-oligothiophenes has also allowed us to realize the selective intensification for the former class of fused systems of additional Raman-active vibrational modes, in the low-frequency region, which are also involved in the overall π-conjugation. Their precise assignment, on the basis of the molecular dynamics DFT calculations, indicates that they arise from totally symmetric collective vibrations mostly located on the sulfur or selenium linkages.

Finally, the downward dispersion of the strongest Raman lines of these heteroacenes with respect to their counterparts in nonfused α-oligothiophenes is in agreement with an increasing degree of π-conjugation. This spectroscopic result is consistent with the existence in these fused heterocyclic systems of a fully planar and rigid π-conjugated path of unsaturated C_{sp^2} atoms, surrounded by several electron-rich and easily polarizable heteroatoms. In this regard, the careful comparison between the topologies of the corresponding doubly occupied molecular orbitals higher in energy evidence the significant contribution by the sulfur or selenium atoms to MOs that otherwise are of almost pure π-nature in α-linked oligothiophenes, so that the view of these heteroacenes simply as "rigidified α-oligoheteroaromatics" may be not adequate at all.

Acknowledgment. Research at the University of Málaga was supported by from the Ministerio de Educación y Ciencia (MEC) of Spain through Projects BQU2003-03194 and CTQ2006-14987-C02-01 and by the Junta de Andalucía for funding our FQM-0159 scientific group. R.M.O. and R.P.O are also grateful to the MEC and Junta de Andalucía, respectively, for their personal doctoral grants. Research at Nagoya University was supported by Grants-in-Aids (Nos. 15205014 and 17069011) from the Ministry of Education, Culture, Sports, Science, and Technology of Japan and SORST, Japan Science and Technology Agency. We also thank JEOL Co. for solid-state ^{13}C NMR measurements.

Supporting Information Available: Figures showing solid-state ^{13}C NMR spectra, TGA results, DSC results, and DFT//B3LYP/6-31G** electronic density contours. This material is available free of charge via the Internet at http://pubs.acs.org.

References and Notes

(1) (a) Harvery, R. G. *Polycyclic Aromatic Hydrocarbons*; Wiley-VCH: New York, 1997. (b) Watson, M. D.; Fechtenkötter, A.; Müllen, K. *Chem. Rev.* **2001**, *101*, 267.

(2) (a) Nelson, S. F.; Lin, Y.-Y.; Gundlach, D. J.; Jackson, T. N. *Appl. Phys. Lett.* **1998**, *72*, 1854. (b) Brédas, J. L.; Calbert, J. P.; da Silva Filho, D. A.; Cornil, J. *Proc. Natl. Acad. Sci. U.S.A.* **2002**, *99*, 5804. (c) Mattheus, C. C.; de Wijs, G. A.; de Groot, R. A.; Palstra, T. T. M. *J. Am. Chem. Soc.* **2003**, *125*, 6323. (d) Bendikov, M.; Duong, H. M.; Starkey, K.; Houk, K. N.; Carter, E. A.; Wudl, F. *J. Am. Chem. Soc.* **2004**, *126*, 7416.

(3) (a) Takahashi, T.; Kitamura, M.; Schen, B.; Nakajima, K. *J. Am. Chem. Soc.* **2000**, *122*, 12876. (b) Anthony, J. E.; Brooks, J. S.; Eaton, D. A.; Parkin, S. R. *J. Am. Chem. Soc.* **2001**, *123*, 9482. (c) Payne, M. M.; Parkin, S. R.; Anthony, J. E. *J. Am. Chem. Soc.* **2005**, *127*, 8028. (d) Swartz, C. R.; Parkin, S. R.; Bullock, J. E.; Anthony, J. E.; Mayer, A. C.; Malliaras, G. G. *Org. Lett.* **2005**, *7*, 3163. (e) Dickey, K. C.; Anthony, J. E.; Loo, Y.-L. *Adv. Mater.* **2006**, *18*, 1721. (f) Perepichka, D. F.; Bendikov, M.; Meng, H.; Wudl, F. *J. Am. Chem. Soc.* **2003**, *125*, 10190. (g) Sakamoto, Y.; Suzuki, T.; Kobayashi, M.; Gao, Y.; Fukai, Y.; Inoue, Y.; Sato, F.; Tokito, S. *J. Am. Chem. Soc.* **2004**, *126*, 8138. (h) Chan, S. H.; Lee, H. K.; Wang, Y. M.; Fu, N. Y.; Chen, X. M.; Cai, Z. W.; Wong, H. N. C. *Chem. Commun.* **2005**, 66.

(4) (a) Dimitrakopoulos, C. D.; Malefant, P. R. L. *Adv. Mater.* **2002**, *14*, 99. (b) Katz, H. E.; Bao, Z.; Gilat, S. L. *Acc. Chem. Res.* **2001**, *34*, 359.

(5) (a) Schroth, W.; Hintzsche, E.; Viola, H.; Winkler, R.; Klose, H.; Boese, R.; Kempe, R.; Sieler, J. *Chem. Ber.* **1994**, *127*, 401. (b) Schroth, W.; Hintzsche, E.; Felicetti, M.; Spitzner, R.; Sieler, J.; Kempe, R. *Angew. Chem., Int. Ed. Engl.* **1994**, *33*, 739. (c) Schroth, W.; Hintzsche, E.; Jordan, H.; Jende, T.; Spitzner, R.; Thondorf, I. *Tetrahedron* **1997**, *53*, 7509.

(6) (a) Mazaki, Y.; Kobayashi, K. *J. Chem. Soc., Perkin Trans.* **1992**, *2*, 761. (b) Sato, N.; Mazaki, Y.; Kobayashi, K.; Kobayashi, T. *J. Chem. Soc., Perkin Trans.* **1992**, *2*, 765.

(7) (a) Zhang, X.; Côté, A. P.; Matzger, A. J. *J. Am. Chem. Soc.* **2005**, *127*, 10502. (b) Malave Osuna, R.; Zhang, X.; Matzger, A. J.; Hernández, V.; López Navarrete, J. T. *J. Phys. Chem. A.* **2006**, *110*, 5058.

(8) Oyaizu, K.; Iwasaki, T.; Tsukahara, Y.; Tsuchida, E. *Macromolecules* **2004**, *37*, 1257.

(9) Other thiophene-based heteroacenes: (a) Li, X.-C.; Sirringhaus, H.; Garnier, F.; Holmes, A. B.; Moratti, S. C.; Feeder, N.; Clegg, W.; Teat, S. J.; Friend, R. J. *J. Am. Chem. Soc.* **1998**, *120*, 2206. (b) Rajca, A.; Wang, H.; Pink, M.; Rajca, S. *Angew. Chem., Int. Ed.* **2000**, *39*, 4481. (c) Rajca, A.; Miyasaka, M.; Pink, M.; Wang, H.; Rajca, S. *J. Am. Chem. Soc.* **2004**, *126*, 15211. (d) Miyasaka, M.; Rajca, A.; Pink, M.; Rajca, S. *J. Am. Chem. Soc.* **2005**, *127*, 13806. (e) Miyasaka, M.; Rajca, A. *J. Org. Chem.* **2006**, *71*, 3264. (f) Zhang, X.; Matzger, A. J. *J. Org. Chem.* **2003**, *68*, 9813. (g) Nenajdenko, V. G.; Sumerin, V. V.; Chernichenko. K. Y.; Balenkova, E. S. *Org. Lett.* **2004**, *6*, 3437. (h) Nicolas, Y.; Blanchard, P.; Roncali, J.; Allain, M.; Mercier, N.; Deman, A.-L.; Tardy, J. *Org. Lett.* **2005**, *7*, 3513.

(10) Werz, D. B.; Gleiter, R.; Rominger, F. *J. Am. Chem. Soc.* **2002**, *124*, 10638.

(11) Okamoto, T.; Kudoh, K.; Wakamiya, A.; Yamaguchi, S. *Org. Lett.* **2005**, *7*, 5301.

(12) (a) Zerbi, G.; Castiglioni, C.; Del Zoppo, M. *Electronic Materials The Oligomer Approach*; Wiley−VCH: Weinheim, Germany, 1998; p 345. (b) Castiglioni, C.; Gussoni, M.; López Navarrete, J. T.; Zerbi, G. *Solid State Commun.* **1988**, *65*, 625. (c) López Navarrete, J. T.; Zerbi, G. *J. Chem. Phys.* **1991**, *94*, 957 and 965. (d) Hernández, V.; Castiglioni, C.; Del Zoppo, M.; Zerbi, G. *Phys. Rev. B* **1994**, *50*, 9815. (e) Agosti, E.; Rivola, M.;

Hernández, V.; Del Zoppo, M.; Zerbi, G. *Synth. Met*. **1999**, *100*, 101. (f) Zerbi, G. *Handbook of Conducting Polymers*; Marcel Dekker: New York, 1998.

(13) Frisch, M. J.; Trucks, G. W.; Schlegel, H. B.; Scuseria, G. E.; Robb, M. A.; Cheeseman, J. R.; Montgomery, J. A., Jr.; Vreven, T.; Kudin, K. N.; Burant, J. C.; Millam, J. M.; Iyengar, S. S.; Tomasi, J.; Barone, V.; Mennucci, B.; Cossi, M.; Scalmani, G.; Rega, N.; Petersson, G. A.; Nakatsuji, H.; Hada, M.; Ehara, M.; Toyota, K.; Fukuda, R.; Hasegawa, J.; Ishida, M.; Nakajima, T.; Honda, Y.; Kitao, O.; Nakai, H.; Klene, M.; Li, X.; Knox, J. E.; Hratchian, H. P.; Cross, J. B.; Adamo, C.; Jaramillo, J.; Gomperts, R.; Stratmann, R. E.; Yazyev, O.; Austin, A. J.; Cammi, R.; Pomelli, C.; Ochterski, J. W.; Ayala, P. Y.; Morokuma, K.; Voth, G. A.; Salvador, P.; Dannenberg, J. J.; Zakrzewski, V. G.; Dapprich, S.; Daniels, A. D.; Strain, M. C.; Farkas, O.; Malick, D. K.; Rabuck, A. D.; Raghavachari, K.; Foresman, J. B.; Ortiz, J. V.; Cui, Q.; Baboul, A. G.; Clifford, S.; Cioslowski, J.; Stefanov, B. B.; Liu, G.; Liashenko, A.; Piskorz, P.; Komaromi, I.; Martin, R. L.; Fox, D. J.; Keith, T.; Al-Laham, M. A.; Peng, C. Y.; Nanayakkara, A.; Challacombe, M.; Gill, P. M. W.; Johnson, B.; Chen, W.; Wong, M. W.; Gonzalez, C.; Pople, J. A. *Gaussian 03*, revision B.04; Gaussian Inc.: Pittsburgh, PA, 2003.

(14) Becke, A. D. *J. Chem. Phys.* **1993**, *98*, 1372.

(15) Stephens, P. J.; Devlin, F. J.; Chabalowski, F. C. F.; Frisch, M. J. *J. Phys. Chem.* **1994**, *98*, 11623.

(16) Novoa, J. J.; Sosa, C. *J. Phys. Chem.* **1995**, *99*, 15837.

(17) Scott, A. P.; Radom, L. *J. Phys. Chem.* **1996**, *100*, 16502.

(18) Rauhut, G.; Pulay, P. *J. Phys. Chem.* **1995**, *99*, 3093.

(19) Francl, M. M.; Pietro, W. J.; Hehre, W. J.; Binkley, J. S.; Gordon, M. S.; Defrees, D. J.; Pople, J. A. *J. Chem. Phys.* **1982**, *77*, 3654.

(20) Runge, E.; Gross, E. K. U. *Phys. Rev. Lett.* **1984**, *52*, 997. Gross, E. K. U.; Kohn, W. *Adv. Quantum Chem.* **1990**, *21*, 255. *Density Functional Theory*; Gross, E. K. U., Driezler, R. M., Eds.; Plenum Press: New York, 1995; p 149.

(21) Casida, M. E. *Recent Advances in Density Functional Methods, Part I*; Chong, D. P., Ed.; World Scientific: Singapore, 1995; p 115.

(22) Koch, W.; Holthausen, M. C. *A Chemist's Guide to Density Functional Theory*; Wiley-VCH: Weinheim, Germany, 2000.

(23) Casado, J.; Miller, L. L.; Mann, K. R.; Pappenfus, T. M.; Kanemitsu, Y.; Ortí, E.; Viruela, P. M.; Pou-Amérigo, R.; Hernández, V.; López Navarrete, J. T. *J. Phys. Chem. B* **2002**, *106*, 3872.

(24) Portmann, S.; Lüthi, H. P. *Chimia* **2000**, *54*, 766−770.

(25) Sakamoto, A.; Furukawa, Y.; Tasumi, M. *J. Phys. Chem*. **1994**, *98*, 4635.

(26) (a) Yokonuma, N.; Furukawa, Y.; Tasumi, M.; Kuroda, M.; Nakayama, J. *Chem. Phys. Lett.* **1996**, *255*, 431. (b) Harada, I.; Furukawa, Y. *Vibrational Spectra and Structure*; Durig, J., Ed.; Elsevier: Amsterdam, 1991; Vol. 19, p 369.

(27) (a) Hernández, V.; Casado, J.; Ramirez, F. J.; Zotti, G.; Hotta, S.; López Navarrete, J. T. *J. Chem. Phys.* **1996**, *104*, 9271. (b) Casado, J.; Hernández, V.; Hotta, S.; López Navarrete, J. T. *J. Chem. Phys.* **1998**, *109*, 10419. (c) Moreno Castro, C.; Ruiz Delgado, M. C.; Hernández, V.; Hotta, S.; Casado, J.; López Navarrete, J. T. *J. Chem. Phys.* **2002**, *116*, 10419. (d) Moreno Castro, C.; Ruiz Delgado, M. C.; Hernández, V.; Shirota, Y.; Casado, J.; López Navarrete, J. T. *J. Phys. Chem. B* **2002**, *106*, 7163. (e) Ruiz Delgado, M. C.; Hernández, V.; López Navarrete, J. T.; Tanaka, S.; Yamashita, Y. *J. Phys. Chem. B* **2004**, *108*, 2516. (f) Ruiz Delgado, M. C.; Casado, J.; Hernández, V.; López Navarrete, J. T.; Fuhrmann, G.; Bauerle, P. *J. Phys. Chem. B* **2004**, *108*, 3158. (g) Casado, J.; Ponce Ortiz, R.; Ruiz Delgado, M. C.; Azumi, R.; Oakley, R. T.; Hernández, V.; López Navarrete, J. T. *J. Phys. Chem. B* **2005**, *109*, 10115.

(28) (a) Casado, J.; Hernández, V.; Hotta, S.; López Navarrete, J. T. *J. Chem. Phys.* **1998**, *109*, 10419. (b) Casado, J.; Hernández, V.; Hotta, S.; López Navarrete, J. T. *Adv. Mater*. **1998**, *10*, 1258. (c) Casado, J.; Miller, L. L.; Mann, K. R.; Pappenfus, T. M.; Kanemitsu, Y.; Orti, E.; Viruela, P. M.; Pou-Amerigo, P.; Hernández, V.; López Navarrete, J. T. *J. Phys. Chem. B* **2002**, *106*, 3872. (d) Casado, J.; Miller, L. L.; Mann, K. R.; Pappenfus, T. M.; Hernández, V.; López Navarrete, J. T. *J. Phys. Chem. B* **2002**, *106*, 3597. (e) Casado, J.; Ruiz Delgado, M. C.; Shirota, Y.; Hernández, V.; López Navarrete, J. T. *J. Phys. Chem. B* **2003**, *107*, 2637. (f) Casado, J.; Hernández, V.; Ponce Ortiz, R.; Ruiz Delgado, M. C.; López Navarrete, J. T.; Fuhrmann, G.; Bauerle, P. *J. Raman Spectrosc*. **2004**, *35*, 592.

(29) (a) Hernández, V.; Casado, J.; Effenberger, F.; López Navarrete, J. T. *J. Chem. Phys.* **2000**, *112*, 5105. (b) Delgado Ledesma, S.; Ponce Ortiz, R.; Ruiz Delgado, M. C.; Vida, Y.; Perez-Inestrosa, E.; Casado, J.; Hernández, V.; Kim, O.-K.; Lehn, J.-M.; López Navarrete, J. T. *Chem.*—Eur. J. **2004**, *10*, 3805.

(30) (a) Gonzalez, M.; Segura, J. L.; Seoane, C.; Martin, N.; Garin, J.; Orduna, J.; Alcala, R.; Villacampa, B.; Hernández, V.; López, Navarrete, J. T. *J. Org. Chem.* **2001**, *66*, 8872. (b) Casado, J.; Pappenfus, T. M.; Miller, L. L.; Mann, K. R.; Orti, E.; Viruela, P. M.; Pou-Amerigo, P.; Hernández, V.; López Navarrete, J. T. *J. Am. Chem. Soc*., **2003**, *125*, 2534. (c) Moreno Oliva, M.; Casado, J.; Raposo, M. M. M.; Fonseca, A. M. C.; Hartmann, H.; Hernández, V.; López Navarrete, J. T. *J. Org. Chem*. **2006**, *71*, 7509.

(31) (a) Ehrendorfer, Ch.; Karpfen, A. *J. Phys. Chem*. **1994**, *98*, 7492. (b) Ehrendorfer, Ch.; Karpfen, A. *J. Phys. Chem.* **1995**, *99*, 5341.